Sondeur multifaisceaux
Dorsale fossile
Mer de Chine méridionale
Analyse structurale
Géodynamique

Seabeam
Fossil ridge
South China Sea
Structural analysis
Geodynamics

The axial ridge of the South China Sea: a Seabeam and geophysical survey

Guy PAUTOT [a], Claude RANGIN [b], Anne BRIAIS [c], Jinlong WU [d], Shuqiao HAN [d], Hengxiu LI [d], Yingxian LU [d], Jicheng ZHAO [d]

[a] Institut Français de Recherche pour l'Exploitation de la Mer (IFREMER), Centre de Brest, B.P. n° 70, 29280 Plouzané, France.

[b] Laboratoire de Géologie Structurale, Université Paris-VI, 4, Place Jussieu, 75252 Paris Cedex 05, France.

[c] Institut de Physique du Globe, Université Paris-VI, 4, Place Jussieu, 75252 Paris Cedex 05, France.

[d] First Institute of Oceanography, National Bureau of Oceanography, PO Box 98, Qingdao, People's Republic of China.

Received 13/3/89, in revised form 13/10/89, accepted 20/10/89.

ABSTRACT

We use observations from the 1985 *R/V Charcot* cruise *Nanhai* to document Northwest-Southeast spreading in the 150-200 km wide axial region of the South China Sea (SCS). The data include Seabeam and single channel seismic profiles, complemented by magnetic and gravity anomalies. Detailed surveys were performed on both sides of the ridge to examine the structural fabric. A fine scale structural survey of the flank of a seamount, performed with a side scan sonar, is also presented, as well as results from dredges and cores. These observations imply that the last stage of spreading in the SCS basin was oriented Northwest-Southeast, and created oceanic crust transected by numerous transform faults trending Northwest-Southeast in the central area. The alkalic lavas forming the Scarborough Seamount chain are injected along the relict spreading axis and N 140°E trending transform faults and are dated 11-6 My. They were probably emplaced at the end of the spreading, and after its cessation. We conclude that the structural fabric of the axial ridge is uniform throughout the South China Sea, and that the spreading in the axis area was probably uniform in time. Along the edges of the surveyed area, rift structures with a different orientation (N 80°E) were also observed. We present two alternative kinematic interpretations for the evolution of the basin. One involves the extrusion of Sundaland along large strike-slip faults in response to the India-Asia collision. Rifts trending ≈ Northeast-Southwest are created at the tips of those faults by Tertiary left lateral motion along them, and the oceanic spreading follows the same structural directions. The second interpretation implies a 20 to 30° counterclockwise rotation of the rift axis, with a general kinematic reorganization around 20 My.

Oceanologica Acta, 1990. **13**, 2, 129-143.

RÉSUMÉ

La dorsale fossile de la Mer de Chine méridionale: une étude morpho-structurale

De nouvelles données ont été obtenues, au cours de la campagne du *N.O. Jean-Charcot* en Mer de Chine méridionale, sur la partie axiale de la dorsale fossile ayant créé le bassin central. Ces données sont des données géophysiques classiques: gravimétriques, magnétométriques et de sismique continue, obtenues simultanément avec des données de sondeur multifaisceaux. Une première phase exploratoire a eu lieu sur 1 000 km d'axe de dorsale par grands profils sécants. Deux zones-clés ont ensuite été étudiées avec un maillage serré pour comprendre la fabrique structurale. Enfin, un profil de sonar latéral a été réalisé, ainsi que des dragages et des carottages.

Notre analyse structurale montre que le dernier stade d'ouverture est une extension orientée Nord-Ouest-Sud-Est. Cette extension a conduit à la création d'une dorsale dont la largeur atteint 200 km, et qui est composée de trois segments juxtaposés. Le segment central est disséqué par plusieurs zones de fracture orientées Nord-Ouest-Sud-Est. La chaîne de volcans Scarborough est disposée préférentiellement sur le segment central et à la jonction de tronçons de rift et de zone de fracture. Ce volcanisme est alcalin et d'âge post-rifting. Les deux autres segments sont plus homogènes. En bordure externe des segments de dorsale, la fabrique structurale devient Est-Ouest. Nous présentons deux interprétations cinématiques alternatives pour décrire l'évolution du bassin. La première implique l'extrusion de la plate-forme de la Sonde le long de failles de coulissage majeures en réponse à la collision Inde-Asie. La seconde est liée à la subduction pacifique et à la rotation de l'archipel philippin, qui entraînent une rotation de 20 à 30°, dans le sens trigonométrique inverse, de l'axe de la dorsale il y a environ vingt millions d'années.

Oceanologica Acta, 1990. **13**, 2, 129-143.

INTRODUCTION

The South China Sea (SCS) is a complex marginal oceanic basin, created by rifting of the Chinese mainland during Paleogene time. It is presently subducting along the Manila trench, a well documented convergent boundary, active from late Tertiary time.

To the South, the rifted continental block, which includes North Palawan, Reed Bank and Dangerous Grounds, is the foreland for the northward thrusting of an island arc terrane, the Cagayan ridge, which collided with this continental margin in middle Miocene time (Holloway, 1982). The Palawan trough is interpreted either as a relict subduction zone, implying that the southern margin of the SCS was formerly active (Taylor and Hayes, 1980; 1983), or as a deep sedimentary graben in a passive margin (Fricaud, 1984; Hinz ans Schlüter, 1985).

East-trending magnetic lineations in the eastern half of the basin date sea-floor spreading as mid-Oligocene through early Miocene (32-17 My; Taylor and Hayes, 1980; 1983). The southwestern abyssal plain of the SCS is less well understood. This part of the basin is considered either as of Cretaceous origin (Ru and Pigott, 1986; Lu *et al.*, 1987), or cœval with the Eastern basin (Hayes *et al.*, 1987).

Different geodynamic models have been proposed to explain the geodynamic evolution of the SCS. These models present various types of mechanisms. One model involves a scissor shape opening of the basin (Ben-Avraham and Uyeda, 1973; Bowin *et al.*, 1978). A second model involves a North-South spreading, based on the direction of the magnetic anomalies. This direction may be related to the subduction in the Palawan trench of a Mesozoic oceanic basin (Taylor and Hayes, 1983; Holloway, 1982; Ru and Pigott, 1986). Peltzer (1983) and Tapponnier *et al.* (1986) related the opening of the basin to the Southeast extrusion of Sundaland in response to the India-Asia collision. Finally, the evidence for a Northeast-Southwest fabric in the axial region of the basin lead Pautot *et al.* (1986) to propose an opening of the basin in two stages, with first North-South, then Northwest-Southeast directions of extension.

In this paper we focus on the last spreading stage of the SCS basin. We present, on the basis of our data, the magnetic and gravity signature of the extinct spreading centre, as well as its morphological and structural pattern, as documented by Seabeam and single channel seismic data. Sediment cores and dredges on seamounts distributed along the axial ridge provide more constraints on the age of the volcanic event. Interpretation of side-scan images of one of the seamounts leads to more accurate models for their emplacement.

METHODOLOGY

The *Nanhai* cruise was devoted to a study of the axial ridge of the South China basin, between 113° and 119°E (Fig. 1). It was the first cruise in the area to record both Seabeam and continuous single channel seismic data. The simultaneous deployment of these devices permits an accurate morphostructural analysis of the seafloor. To take advantage of the Seabeam's resolution, we focused the profiles on the central part of the basin, where the ridge is not buried by thick sediments (< 1 000 m thick). Off-ridge, the sediments are thicker (1 000-2 500 m), and tend to smooth the scarps, making morphologic analysis more difficult. A total of 74 profiles, spaced along the 1 000 km long axial ridge, were obtained.

In addition to the seismic and Seabeam observations, gravity and magnetic profiles were also recorded, providing information on the age and evolution of the oceanic crust (Fig. 2 and 3).

Rock dredges and sediment cores were also taken at the top of three of the axial seamounts and in the abyssal plain, providing constraints on the age of the volcanic event and the sedimentological history of the basin.

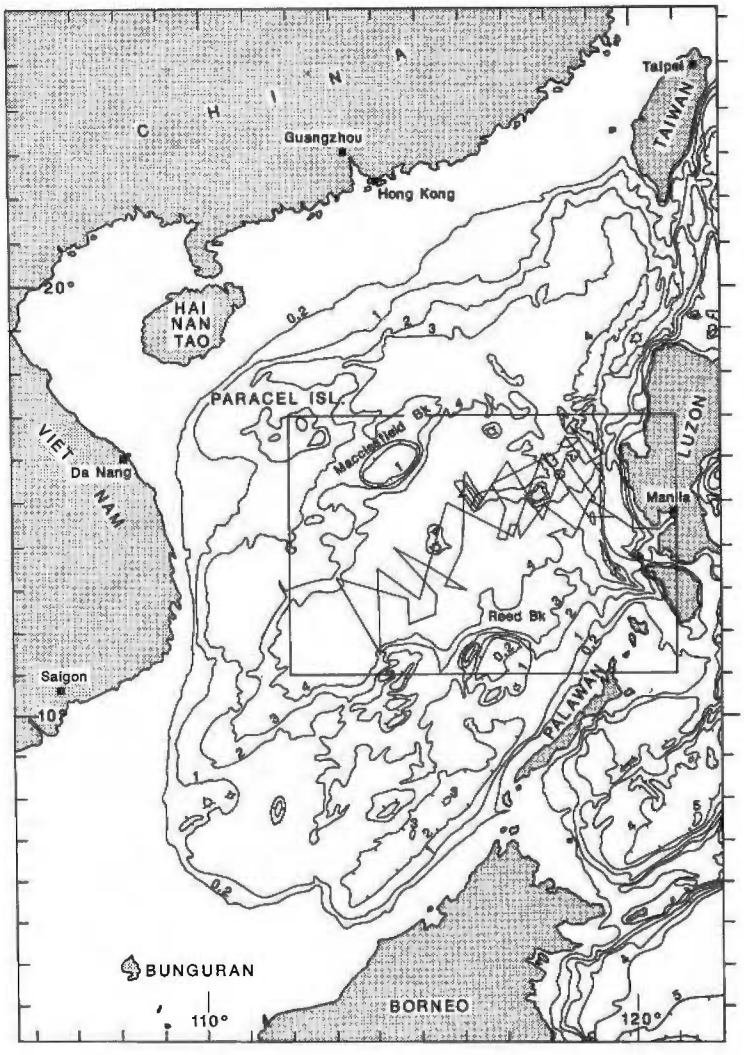

Figure 1

Bathymetric map of the South China Sea showing the ship tracks of Nanhai *cruise. Contours in kilometres. Box shows location of Figures* 2 *and* 3.

Carte bathymétrique simplifiée de la Mer de Chine méridionale, portant le parcours du navire au cours de la campagne *Nanhai*. Les lignes isobathes sont exprimées en kilomètres. Le rectangle délimite la zone d'étude et le cadre des figures 2 et 3.

One of these seamounts was the site for a first test of the new French deep-towed side-scan sonar (SAR: "système acoustique remorqué"; Fig. 9).

GEOPHYSICAL DATA

The free-air gravity anomalies plotted along tracks are shown in Figure 2. In the southwestern part of the study area, a gravity low clearly appears associated with the relict spreading axis (Taylor and Hayes, 1983).

On the easternmost profiles, the active subduction zone of the Manila trench is outlined by a −120 mgal gravity low, which corresponds to the location of the trench on the Seabeam swaths and on the seismic profiles.

In the central area, the Scarborough seamounts are associated with 50-100 mgal high gravity anomalies. These features "overprint" any possible low related to the relict spreading axis. On one profile however, the axis can be located, near 15°N,117° E (Fig. 2). On two more easterly profiles, the topography, especially the inward-facing normal faults scarps, allow us to locate the spreading axis at a point corresponding to a gravity high symmetrically surrounded by two lows (profiles 3 and 57, Fig *b* 2). We interpret this signature as a gravity high, caused by the axial volcanism observed on the seismic line, which disrupts a broad gravity low associated with the spreading axis. Throughout the eastern part of the basin, the seamounts appear to be preferentially emplaced on the zone of weakness created by the relict spreading axis (Briais *et al.*, in press).

The southwestern abyssal plain displays the most typical gravity profiles. The prominent −25 to −30 mgal lows plotted on profiles, 7,8 and 10 reveal a linear of the ridge trending N 50° E. Southwest and Northeast of this linear section, the ridge axis seems to be offset, respectively left and right laterally, by about 15 km. On profile 14, the same symmetrical seamount signature as on profiles 3 and 57 in the Northeast is observed. The

seamount is thus probably located on the relict axis.

Figure 3 shows the magnetic anomalies plotted along track. The southwestern part of the South China basin is more readily interpreted than the northeastern sub-basin.

If the gravity low is the location of the spreading axis, a preliminary identification of the magnetic anomalies can be performed (Fig. 3). Our model, based on the geomagnetic time scale of Patriat (1983), involves an symmetrical spreading ridge, the half spreading rate (HSR) being slightly higher on the northern limb than on the southern one. Using a HSR of 1.7 cm/yr in the south and 2.0 cm/yr in the north provides an acceptable fit to anomalies 5 *d* to 6, implying an age of 20 (anomaly 6) to 16.5 My (anomaly 5 *c*) for the southwestern basin, as previously suggested by Hayes *et al.* (1987). The magnetic lineations obtained with this model, and their offset along inferred transform faults are in very good agreement with the structure of the ridge revealed by the gravity anomalies (Fig. 2). Because of the shortness of the profiles, this interpretation cannot be used as a definite constraint. Four other sets of anomalies (8-13, 13-18, 20-24 and 27-30) have shapes similar to those observed in the sub-basin. The anomalies 8-13 model would imply an early Oligocene (28-36 My) age, the 13-18 model a late Eocene (36-42 My) age, the 20-24 model an early Eocene (43-53 My) age, and the 27-30 one a Paleocene (60-64 My) age for the southwestern basin. Regardless of the age of the anomalies, the orientation of the magnetic lineations indicates that the direction of spreading in the southwest basin was Northwest-Southeast.

The Eastern sub-basin is much more complex. The magnetic lineations interpreted by Taylor and Hayes (1983) are shown in Figure 3. In the southern flank of the ridge, our observations on closely spaced profiles do not fit their anomaly 6 *a* lineation wery well. On the northern edge of the ridge, anomalies 6 and 6 *a* can be recognized, but here again the correlations are tenuous. Clearly, the spreading history in this area is complex, and probably involves several distinct ridge segments separated by transform faults. As we discuss in the structural study, it seems likely that the direction of these axis segments varied in time by as much as 10 to 15°.

The oceanic crust in the whole surveyed area was probably formed during the same episode of spreading, the last one in the South China Sea, from 20 to 16 My B.P., corresponding to anomalies 6-6 *a* to 5 *d*-5 *c*.

BATHYMETRY AND STRUCTURE OF THE SOUTH CHINA SEA AXIAL RIDGE

Three distinct sections have been identified along the axis of the SCS, each with its own morphological and structural signature: Southwest and Northeast sections are simple linear features that bracket the complex seamount-ridden central section. After presenting the

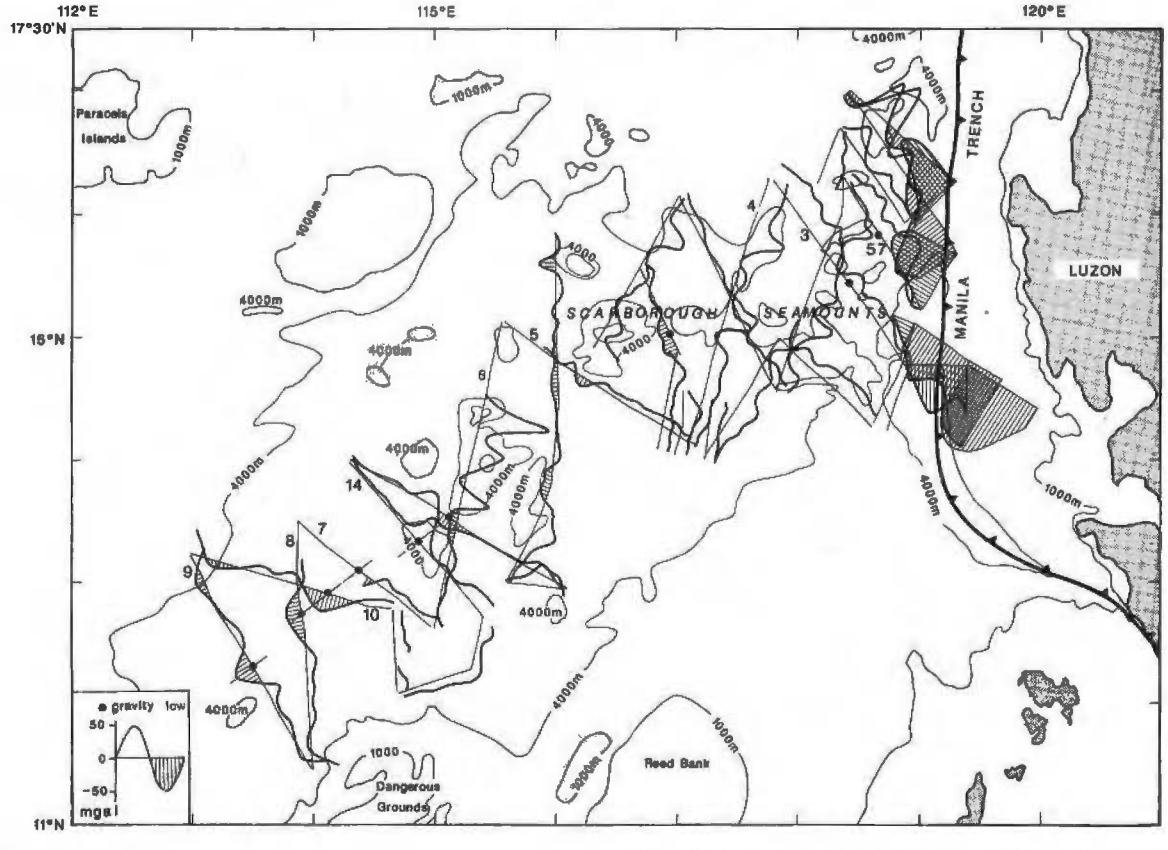

Figure 2

Free-air gravity anomalies projected along track. the axial low gives the location of the relict spreading ridge axis. Numbered profiles are those described in the text.

Anomalies du champ de gravité (air libre) projetées le long du parcours du navire. Le numéro des profils est indiqué. Le minimum observé au centre des profils (et hachuré) correspond à l'axe de la dorsale fossile.

characteristics common to all three sections, we describe each one individually.

Regional characteristics

Morphology and structure of the ridge

Most of the normal faults near the ridge axis trend N 60°E to N 50°E, while off the axis scarps clearly trend N 80°E to N 85°E (Fig. 4). Most of these scarps are imaged on seismic profiles as normal faults boundings outward-tilted blocks (Fig. 5). Horst and graben structures are also observed (profiles 5 and 7 on Figure 5). The relict spreading centre is generally characterized by an axial graben (profiles 5, 7 and 8 on Figure 5) locally invaded by post-spreading seamounts (*see* profile 3 on Figure 5). High energy flat reflectors are observed on seismic profile 9 (Fig. 5), below a transparent seismic sequence which might be pelagic. They form a plateau-like structure extending to both sides of the axis of the ridge. The question remains whether this structure represents fluid lava flows (sheet flows) similar to those present at the crest of the East Pacific rise (Rangin and Francheteau, 1980) and is thus related to spreading; or whether it is composed of coarse-grained turbidites post-dating the spreading history.

Sediment infill

Sediments are irregularly distributed along the extinct spreading centre. Average sediment thickness increases from — 500 m in the Northeast, near the ridge, to 1 000-1 500 m toward the southwestern abyssal plain. The absence of a noticeable variation of the depth of the mudline with the age of the seafloor suggests that the axial ridge is buried by post-spreading sediments.

The thickness of these sediments increases significantly toward the seamounts, indicative of lithospheric flexure in response to the seamount load (*see* profile 4 on Figure 5). The distribution of the seismically transparent sequences (interpreted as hemipelagic sediments) and of the high energy seismic sequences (interpreted as turbidites) is not uniform across the axis of the basin. Turbidites are present mainly in the Southwest section of the ridge, suggesting that their provenance is in mainland China and Indochina. In the eastern section of the ridge, turbidites are also present at the base of the sequence in direct contact with the acoustic basement, and are overlaid by a pelagic sequence.

The Southwest and Northeast linear sections

The Southwest sub-basin

The oceanic floor shows essentially the same fabric throughout a 170 km wide axial strip. This observation

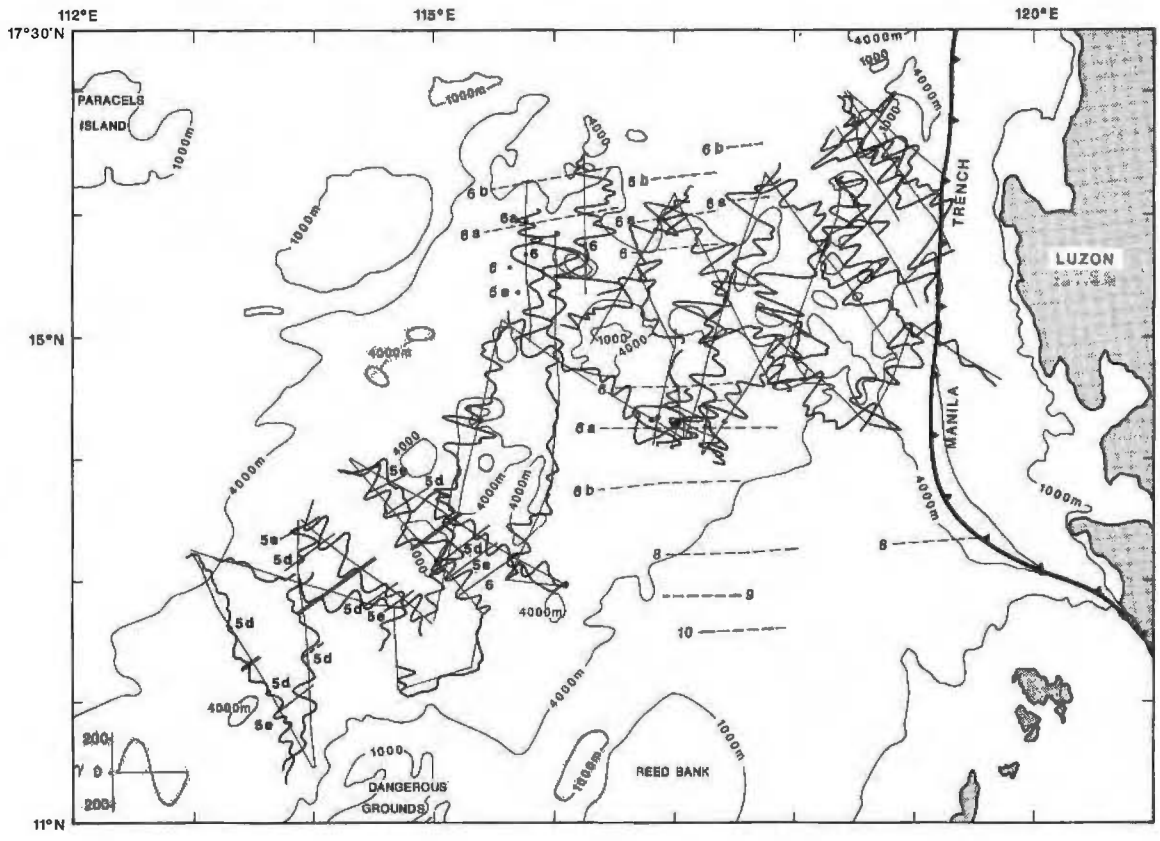

Figure 3

Magnetic anomalies projected along track and primary correlations, with the 6-5 d model in the Southwestern basin. Anomalies recognized by Taylor and Hayes (1983) *shown in dotted lines.*

Anomalies du champ magnétique projetées le long du parcours du navire. Les corrélations présentées sont celles retenues avec le modèle 6-5 *d* dans le bassin Sud-Ouest. Les anomalies antérieures à 6 *a* sont représentées en tirets, et ont été identifiées par Taylor et Hayes (1983).

does not support the scissor-shape opening model for this basin, proposed by Ben-Avraham and Uyeda (1973) and Bowin *et al.* (1978).

The crustal Continent-Ocean Boundary (COB) is visible on various profiles along flanks of the ridge (*see* profile 9 on Figure 6). Here the continental crust, marked by elevated and highly sedimented tilted blocks, contrasts with the bumpy, deep and moderately sedimented acoustic basement of the oceanic crust (*see* Fig. 6). The COB is also outlined by a strong contrast of the free-air gravity anomaly across both domains (Fig. 6). Along this ridge section, the structural fabric trends consistently N 55°E. We do not observe transform faults corresponding to the small offsets in the gravity minima, probably due to the sparse Seabeam coverage.

The Northeast section

It is dominated by a structural fabric trending N 50°E, although some graben trending N 80-85°E also occur along the outer flanks of the ridge.

Subduction of the ridge was previously described by Pautot and Rangin (1989) and will not be described in detail here (Fig. 12). The flexure of the downgoing plate is small, and the size and elevation of the axial seamounts decrease toward the trench. The North-South trending deforming front of the accretionary prism is vertically offset by N 130°E trending faults, interpreted as former fracture zones. A large seamount on the northern flank of the ridge, close to the trench axis, was probably emplaced along the ridge jump boundary, as evidenced by its Northeast elongation (Fig. 4).

The central section

The Seabeam swaths in the area between 115°50'E and 118°45'E do not show the typical rift structures seen in the other two sections. The axis of the ridge is very irregular and invaded by large seamounts forming the Scarborough seamount chain. Most of the seamounts are elongated both in the direction of the ridge segments (N 50°E) and along the transform faults direction (N 140°E), suggesting that their growth was controlled by the pre-existing fractures in the oceanic crust (Batiza an Vanko, 1983). This pattern may reveal the presence of a large number of closely-spaced transform faults accommodating a right lateral offset of the ridge axis between the Northeast and Southwest sections (Fig. 4; Pautot *et al.*, 1986; Briais *et al.*, in press).

The *Nanhai* cruise data set is insufficient to constrain the detailed structure of this central section, but detailed surveys performed on both sides of the ridge at the junction of the Southwest and central sections illustrate the structural fabric of this complex area (Fig. 4).

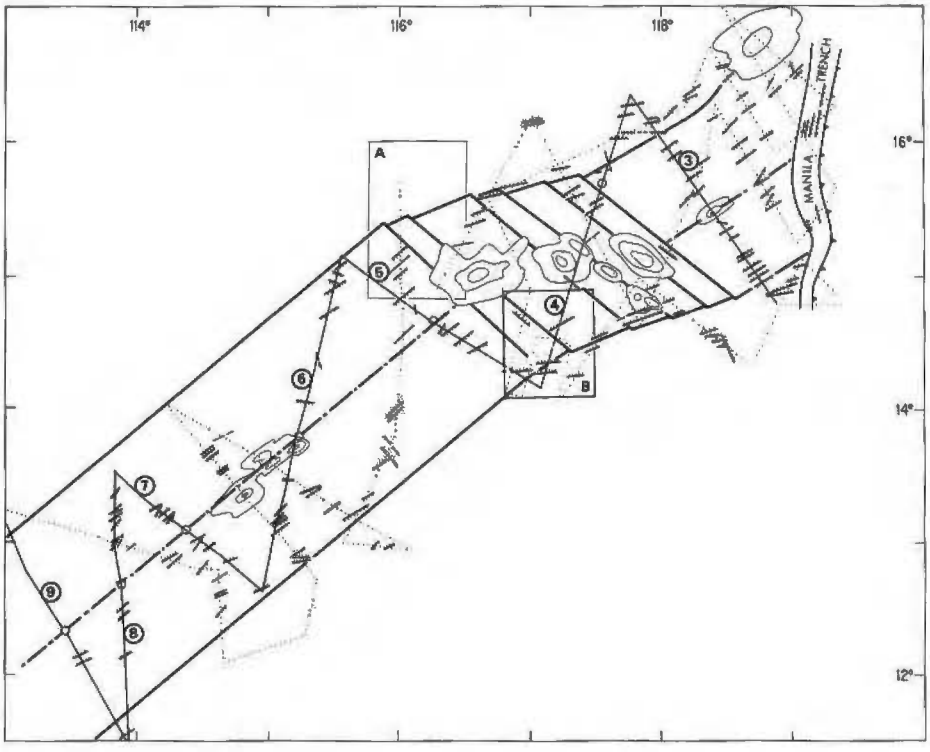

Figure 4

Structural sketch map of the SCS axial ridge (modified from Pautot et al., 1986). Strike and dip of major faults derived from combined analysis of Seabeam and seismic reflection records. Dotted lines are ship tracks. Boxes A (Fig. 7) and B (Fig. 10) are the northern and southern detailed study areas respectively. Thin contours represent major seamounts (Scarborough chain). Thick dashed lines indicate outer limit of zone with predominant N 50°E trending scarps. Dash-dot line outlines probable location of spreading axis.

Représentation structurale de la partie centrale de la dorsale fossile (modifiée de Pautot *et al.*, 1986); les profils sont représentés en traits pleins numérotés et en pointillés. Les édifices volcaniques majeurs sont représentés en traits continus fins. Les rectangles A et B représentent les zones d'étude détaillée présentées sur les figures 7 et 10. La direction et le regard des failles sont représentés le long des profils. La ligne centrale en points-tirets souligne l'axe de la dorsale fossile. L'enveloppe externe des escarpements à orientation N 50°E est matérialisée par un trait continu gras.

The northern detailed survey

The bathymetric map of the survey conducted in the 1° × 1° area illustrates the relationships of the Scarborough seamounts with the fabric of the underlying oceanic crust (Fig. 7). The spreading fabric of the crust is clearly marked by normal faults trending N 50°E and facing Southeast, bounding tilted blocks visible in the southwestern part of the map (Fig. 7 and 8 *a*). Elsewhere, the survey area is blanketed by sediments thicker than in other axial sections of the ridge. A total sediment isopach map for this area shows up to 1.4s (two way travel time; = 1 400 m) thick sediments around the seamounts (Briais *et al.*, in press).

The base of the seamount's slope is marked by a high energy seismic sequence vanishing toward the basin, which could represent a hyaloclastic apron with interbedded sheet lava flows (Fig. 8 *b*). This sequence is topped by the same, but thicker, succession of hemipelagic and turbiditic sediments observed on other parts of the ridge. The onlap of the hemipelagic sediments onto the flanks of the seamounts is clearly shown on profile 41, Figure 8 *b*. Reflective layers in the seismic profile reveal that the bedding in the relatively thick basin sequence is horizontal. If the trough around the seamounts is induced by the flexure of the oceanic lithosphere in response to the volcanoes' load, the absence of tilting of the infilling sequence suggests that this flexure was formed before the deposition of the basin sequence. Toward the center of the basin, this sequence directly overlies the acoustic basement, suggesting that the growth of the volcanic edifices and the subsequent flexure of the lithosphere occurred shortly after cessation of spreading.

This small survey mapped seamounts whose flanks reveal two specific lineations (Fig. 7): 1) the southernmost seamount is roughly aligned with the rift structures (N 50°E); 2) the other seamounts located to the northwest are elongated with a N 130°E trend.

A short-range side-scan sonar (SAR) survey was conducted along the flank of one of these volcanes (Hu Die Feng), elongated in a N 130°E trend (Fig. 9). The SAR images a 500 m wide strip on each side on the track, and coupled 3.5 kHz provides the characteristics of the sediments. In the basin itself, the bottom is flat without any significant features, and the sediments are homogeneous with clear bedding. In a few localized areas the superficial sediments show high reflectivity in small ponds.

The first relief to be detected by SAR at the southern tip of the seamount is associated with volcanic lobated flows which do not show any preferential trend (Fig. 9 *b*. 1). The corresponding 3.5 kHz record clearly shows sediments overlapping the acoustic basement. The flank of this seamount was also imaged (Fig. 9 *b*. 2). The lower slope is covered by a thin veneer of sediments. On the upper part of seamount, no linear features are observed, and the seafloor is rough and devoid of sediments. In the middle of the slope, a 30 m-high cliff trends N 120°E, parallel to both the slope isobaths and the crest of the seamount.

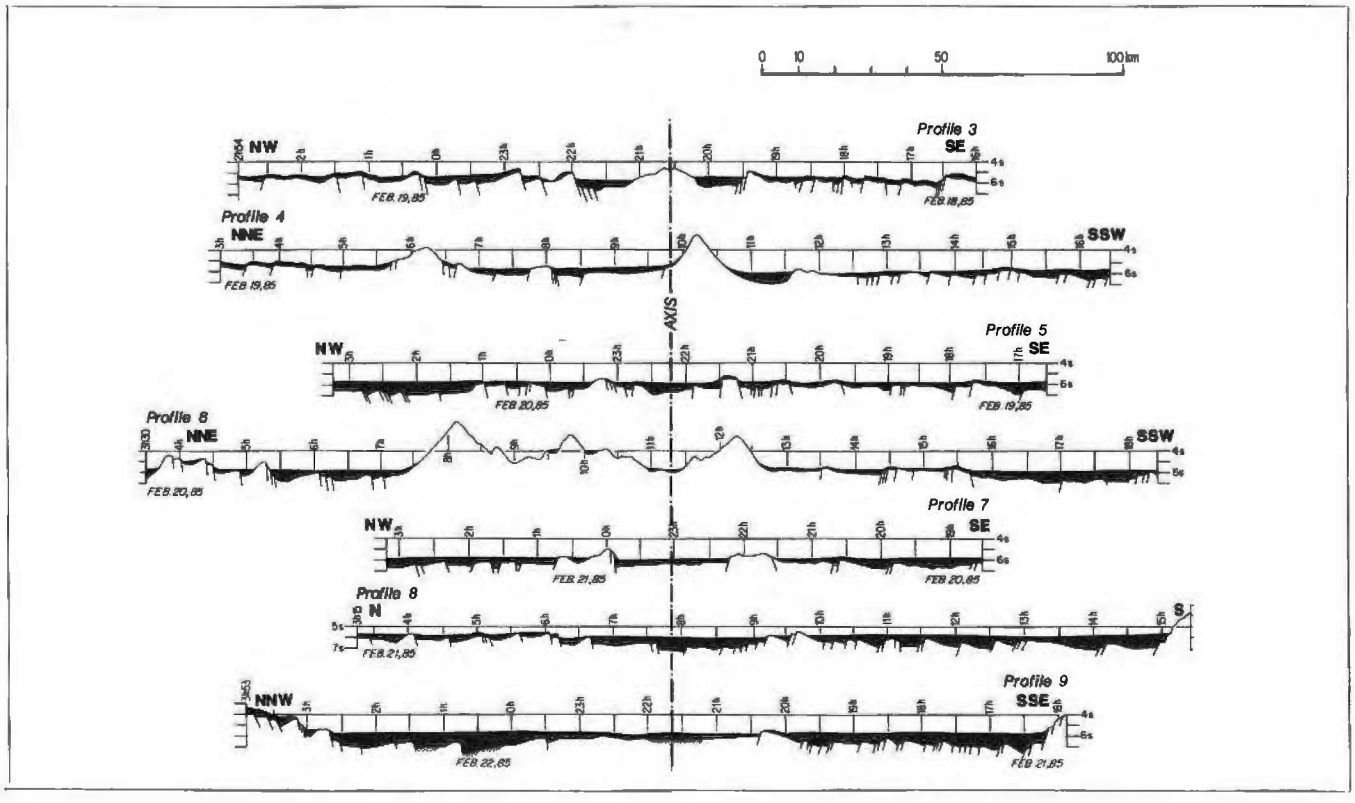

Figure 5

Interpreted single channel profiles across the axial ridge. Sediments covering acoustic basement are shown in black. Vertical scale in seconds (two way travel time).

Interprétation sommaire des profils de sismique continue (canon à eau), représentés en lignes continues sur la figure 4. Les sédiments recouvrant le substratum sont représentés en noir. L'échelle verticale est exprimée en secondes (temps double).

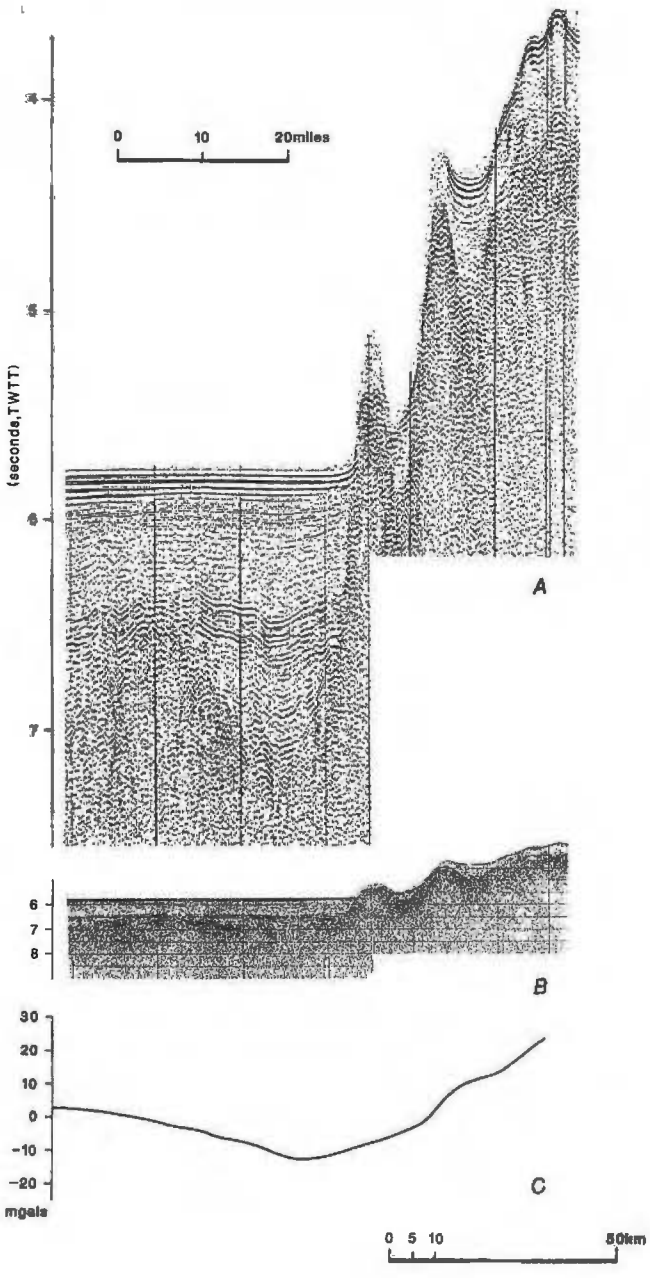

Figure 6

Single-channel profile 9 showing the continental-oceanic crust boundary in the southwestern branch of the South China Sea (location Fig. 2). Steep scarps and tilted continental blocks contrast with the flat oceanic acoustic basement. Vertical exageration for seismic profiles A and B are 15 and 3 respectively. Free-air gravity anomaly across the boundary is shown in profile C.

Profil de sismique continue n° 9 (localisation fig. 2 et 4): contact entre la marge indochinoise et le bassin Sud-Ouest. Les escarpements et les blocs en gradins de la marge contrastent avec le substratum océanique moins accidenté. L'exagération verticale du profil A est de 15, celle du profil B est de 3. Le profil C représente l'anomalie de gravité à l'air libre sur cette zone frontière.

The cliff is transected by N 45°E trending lines, perpendicular to the line of steepest descent. These features could be fissures or small channels in the seamount slope. If the observed lines are really fissures, the flank of the seamount exhibits two structural trends. One strikes parallel to the seamount crest and the second is normal to its elongation direction (N 50°E). The fact that these structures are still observable suggests that this type of seamount was built while the spreading centre was still active, or that they were created during a phase of rejuvenation.

Many of the volcanoes exhibit the same two structural trends at a larger scale in the Seabeam data. As we interpret the general N 130°E trend as the direction of the transform faults and N 50°E one as the ridge crest fabric, it is significant that no East-West or North-South lineations were detected here. The seamounts are here interpreted as injected along the N 50°E trending rift structures, cross-cut by numerous N 130°E trending fracture zones. The presence of these fracture zones could explain the en echelon pattern of the major volcanoes, resulting in the global Est-West trend of the Scarborough seamount chain. Such transform faults are also suggested by the offsets in the magnetic anomaly pattern and the free-air gravity map of the detailed area.

The southern detailed survey

The previously described transform fault system, along the northeastern flank of the ridge, should also be present along its southern flank, but the southern detailed survey reveals an even more complex fabric of the crust (Fig. 10, 11).

This small area is characterized by elongated but discontinuous ridges and basins (Fig. 10). The saddles between the small ridge segments are completely blanketed by recent turbidites. Prominent variations in the seismic sequences thickness are visible on both sides of these ridges, and a good correlation of these seismic sequences can be made along strike (Fig. 11). This suggests that the clastic infilling of these small depocentres occurred axially, and that a limited connection between the different basins existed across strike.

The connections between the depocentres cannot be drawn as straight lines, but imply systematic right lateral offsets (Fig. 10 *a*). These offsets could be due to the presence of transform faults slightly displacing corresponding ridges (Fig. 10 *b*). However the Seabeam data in this area do not show such transform faults. Another way to reconcile the discontinuity of the basins and ridges with the lack of prominent transform faults is to suggest that the troughs and ridges are formed by the succession of small overlapping spreading centres (OSC) creating basins and ridges with sigmoidal shapes (Fig. 10 *c*). The largest relief fault block trends 85°. Several basins and highs further south trend 80°.

Towards the axis of the fossil ridge in this detailed area, some scarce but significant transverse structures with a N 140°E trend can be identified in the Seabeam data (Fig. 10 *a*). The southern detailed study area is characterized by a progressive but distinct change in the strike of the rift structures, from N 80°E off axis to N 50°E near the rift axis. Variations in the trend of the rift structures (N 80°E to N 50°E) support the hypothesis of spreading reorganization of the South China Sea basin (Pautot *et al.*, 1986; *see* discussion below).

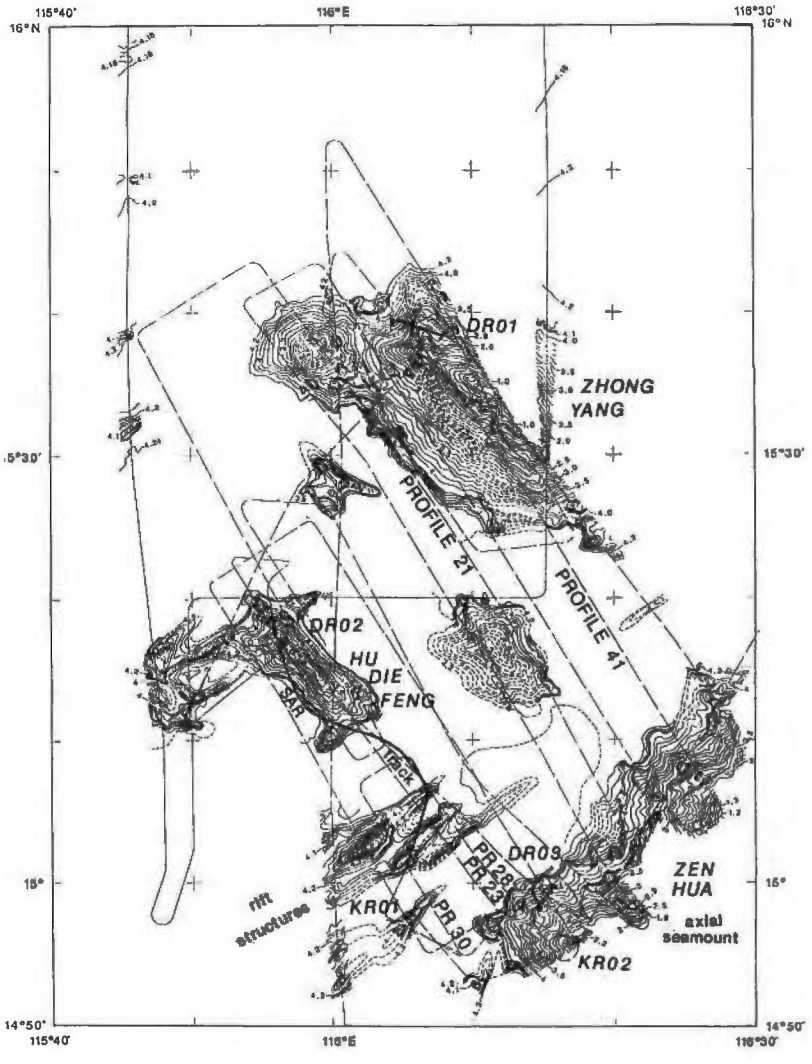

Figure 7

Seabeam bathymetric map of the northern detailed study area, showing seamounts elongated in N 130°E and N 50°E trends, and oceanic crustal fabric characterized by N 50°E trending ridges bounded by normal faults. Dotted line is the Nanhai survey. Continous line is the Masin survey. Dredge and core sites are indicated, as is the SAR track.

Carte seabeam avec position des profils de la zone A (position sur fig. 4). Les montagnes sous-marines montrent des allongements conjugués N 130°E et N 50°E. La fabrique crustale (dans le coin sud-ouest) est clairement N 50°E. La position des carottages (KR), des dragages (DR) et d'un parcours de sonar latéral (SAR) est indiquée.

DREDGING AND CORING RESULTS

Prior to the *Nanhai* cruise, only three seamounts had been dredged successfully during the 1979 *Vema* 36 cruise (Taylor and Hayes, 1983). *Vema* 36-D8 was located close to magnetic anomaly 8. *Vema* 36-D10 was from a seamount located at the axis of the southwestern section of the extinct ridge. *Vema* 36-D9 was from a seamount at the western end of the Scarborough seamount chain. The dredged rocks are typically moderately weathered Mg-coated pillow fragments. They range from aphyric and moderately vesicular (D 10) to phyric and sparsely vesicular. Their major element chemistry identifies them as basalts transitionnal between tholeitic and alkalic. Their petrochemistry is similar to that of the other alkalic and transitional basalts dredged from seamounts formed at the spreading centres of major ocean basins (Taylor and Hayes, 1983).

During the *Nanhai* cruise we also dredged three seamounts in the northern detailed survey box (Fig. 7):

1) NAN-DR0 is located on a large elongated seamount trending Northwest to the North of the Scarborough chain.

2) NAN-DR2 is located on the Hue Die Feng seamount described above.

3) NAN-DR3 is on the same seamount as *Vema* 36-D9.

These rocks belong to the alkalibasalt-trachybasalt series. Most of the samples are highly vesiculated, often irregularly shaped. The rocks are all abundantly coated with Fe-Mn incrustations. A few of them show a slightly curved surface and faint radial jointing, with some fragmented tubes and/or bulbous type of pillow flows, suggestive of pillow-lava shapes. The NAN-DR2 dredge at the seamount crest reveals vesicular, semi-glassy, Fe-Mn coated pillow basalts.

These rocks are alkalic olivine basalts with olivine crystal agglomerates.

Based on the texture, mineralogical variation and chemical composition of their glassy margins, the samples are classified into four categories (Hekinian *et al.*, 1988):

1) Alkali olivine basalts (NAN-DR2).

2) Alkali Olivine plagioclase basalts (NAN-DR1).

3) Alkali highly phaneritic plagioclase basalts (NAN-DR1).

4) Trachybasalts (NAN-DR1 and DR3).

Complementary dredging was performed during the French cruise *Estase*, on a seamount located at the eastern end of the Scarborough seamount chain,

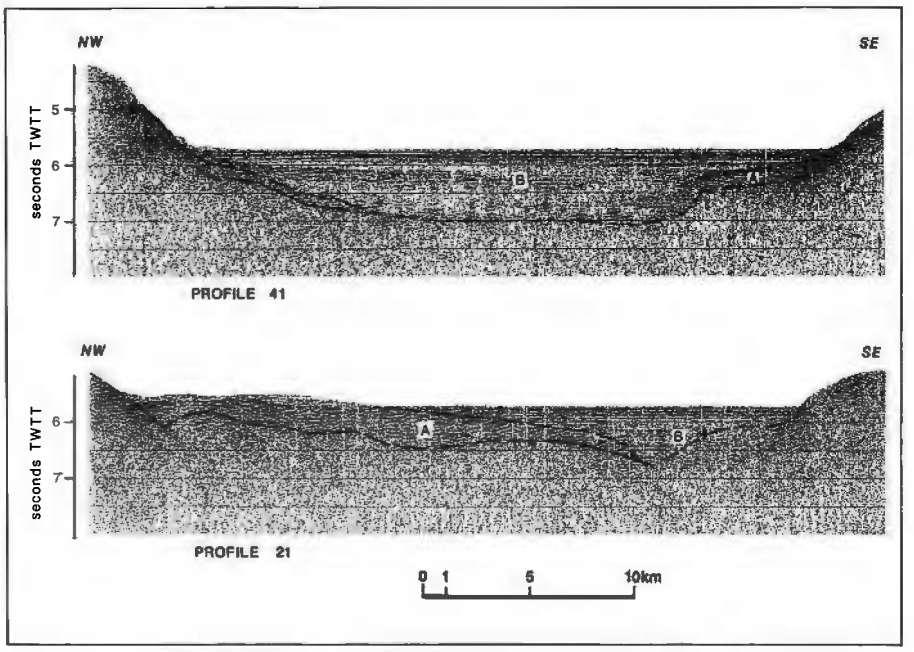

b

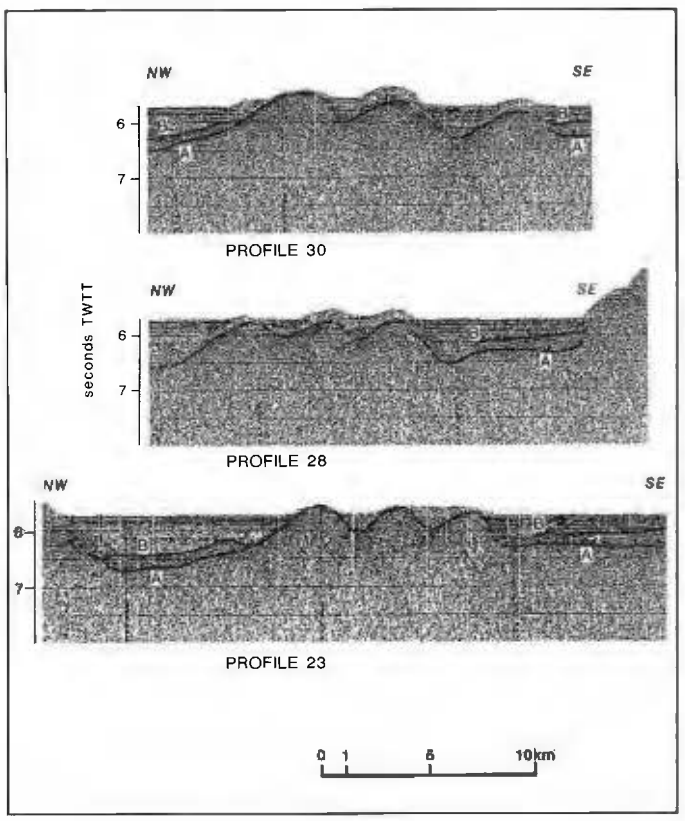

a

Figure 8

Interpreted single-channel seismic lines across the northern detailed area (location Fig. 7).

8 *a: Tilted blocks of oceanic crust in the southwestern part of the area. Same seismic sequences as in Figure* 8 *b.*

8 *b: Volcanic clastic apron (seismic sequence A), onlapped by seismically transparent sequence B, along the flank of the major seamount.*

Représentations des trois profils de sismique continue dans la zone A (position des profils sur la fig. 7).

8 *a* : blocs asymétriques de croûte océanique dans la partie sud-ouest de la zone étudiée. Deux séquences sédimentaires peuvent être individualisées: A: série volcanoclastique; *b* : série acoustiquement transparente, recouverte par une série litée.

8 *b* : flanc d'une montagne sous-marine (mêmes séquences sédimentaires que précédemment).

280 km east of NAN-DR3, where the ridge enters the subduction zone (Hekinian *et al.*, 1988). The dredge contains boulders of volcanic and scoriaceous fragments of trachytic rocks, with a few hyaloclastites and a fragment of aphyric pillow basalt flow. Besides the trachytes, the fragments belong to the different types of lavas recognized in the *Nanhai* samples.

A relationship seems to prevail, not only among the samples collected from the same site, but also among those collected from different sites, which suggests that the dredged rocks might be cogenetic. The least-evolved olivine alkalic basalt was found in NAN-DR2 and the trachyte flow near the trench was petrographically the last eruptive phase observed. All the samples could have been derived from the partial melting of a similar mantle source material (probably garnet lherzolite), suggesting that fractional crystallization during upwelling was the main differentiating process involved.

No genuine tholeiitic basalt was sampled from the different seamounts emplaced on SCS oceanic crust. No clear distinction can be made between seamounts located on the extinct ridge axis and those off axis.

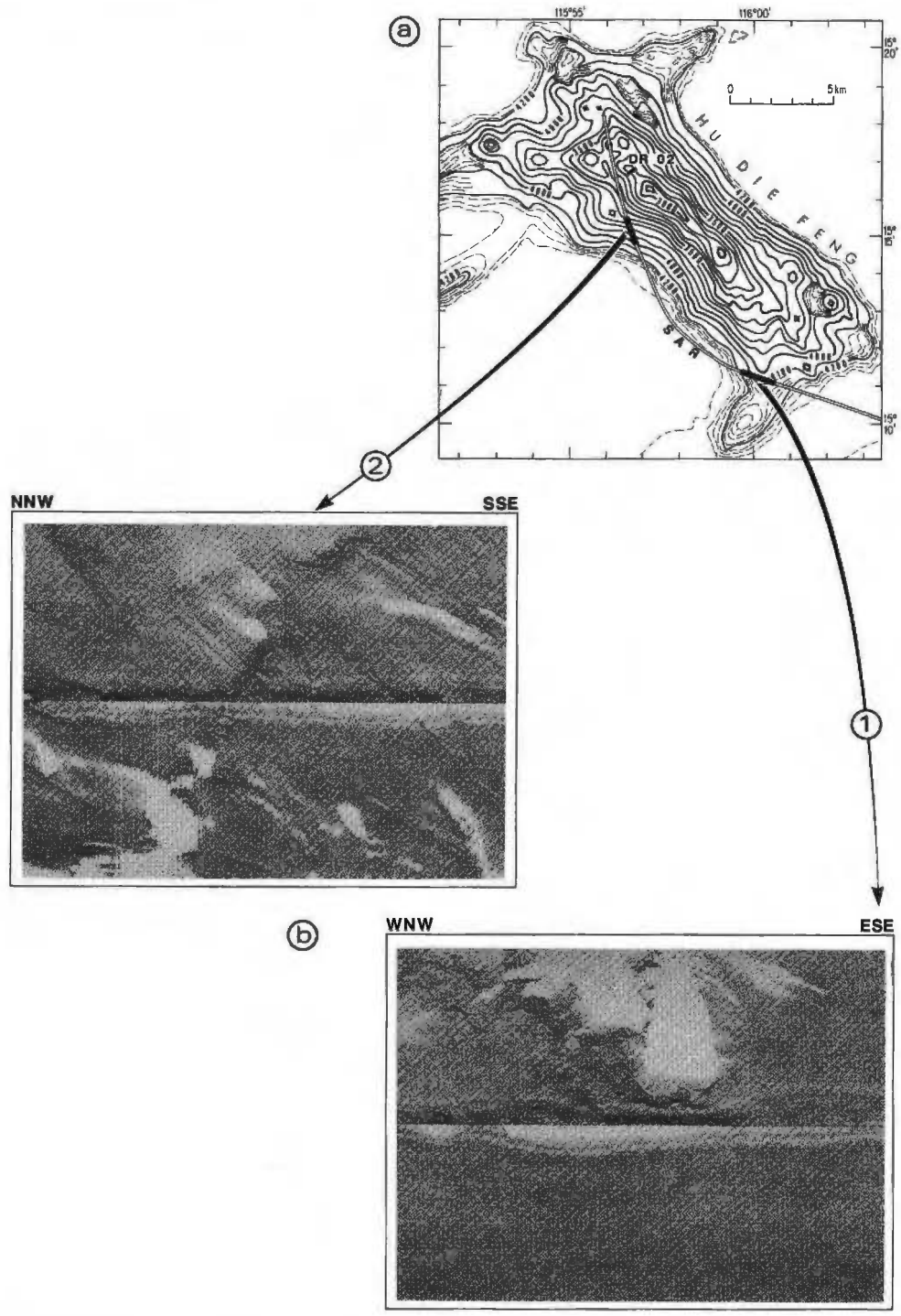

Figure 9

SAR fine scale structure of the central seamount.
a: Bathymetric map of the Hue Die Feng seamount showing location of SAR track and dredge site DR02. SAR was towed from Southeast to North.
b: SAR record along the flank of the seamount: 1) *volcanic lobated side flows;* 2) *major N 130°E trending scarp crossed by N 50°E fractures or channels.*

Images du sonar latéral SAR sur le flanc d'une montagne sous-marine (position fig. 7).
a : carte bathymétrique du mont Hu Die Feng, sur laquelle sont reportés le parcours du SAR et la position du dragage DR2.
b : images du SAR (largeur totale: 1000 m). 1: coulées volcaniques lobées; 2: escarpement majeur orienté N 130°E disséqué par des fractures orientées N 50°E.

At both ends of the Scarborough seamount chain, ages based on nannoplankton were obtained from indurated sediments and hyaloclastites on seamount slopes. The sample from the seamount close to the trench axis gave an early late Miocene age (11 to 8 My: NN9-NN10 nannozones). On the western end of the volcanic chain, a similar sample (in core KS02 close to NAN DR3) contains a nannofossil association of the NN11 zone (upper part of late Miocene: 8 to 6 My). Older sediments, of early middle Miocene age, were dredged during the 1987 *Sonne* cruise (Kudrass, pers. comm.).

If the last event of axial magmatism occured 11 to 8 My ago, as suggested by the dredged sediments, the SCS axis remained hot a long time after the spreading ceased (anomaly 5C, 16 My). These alkalic volcanic lavas were injected probably first during spreading, along active transform and rift structures, but also after the cessation of spreading.

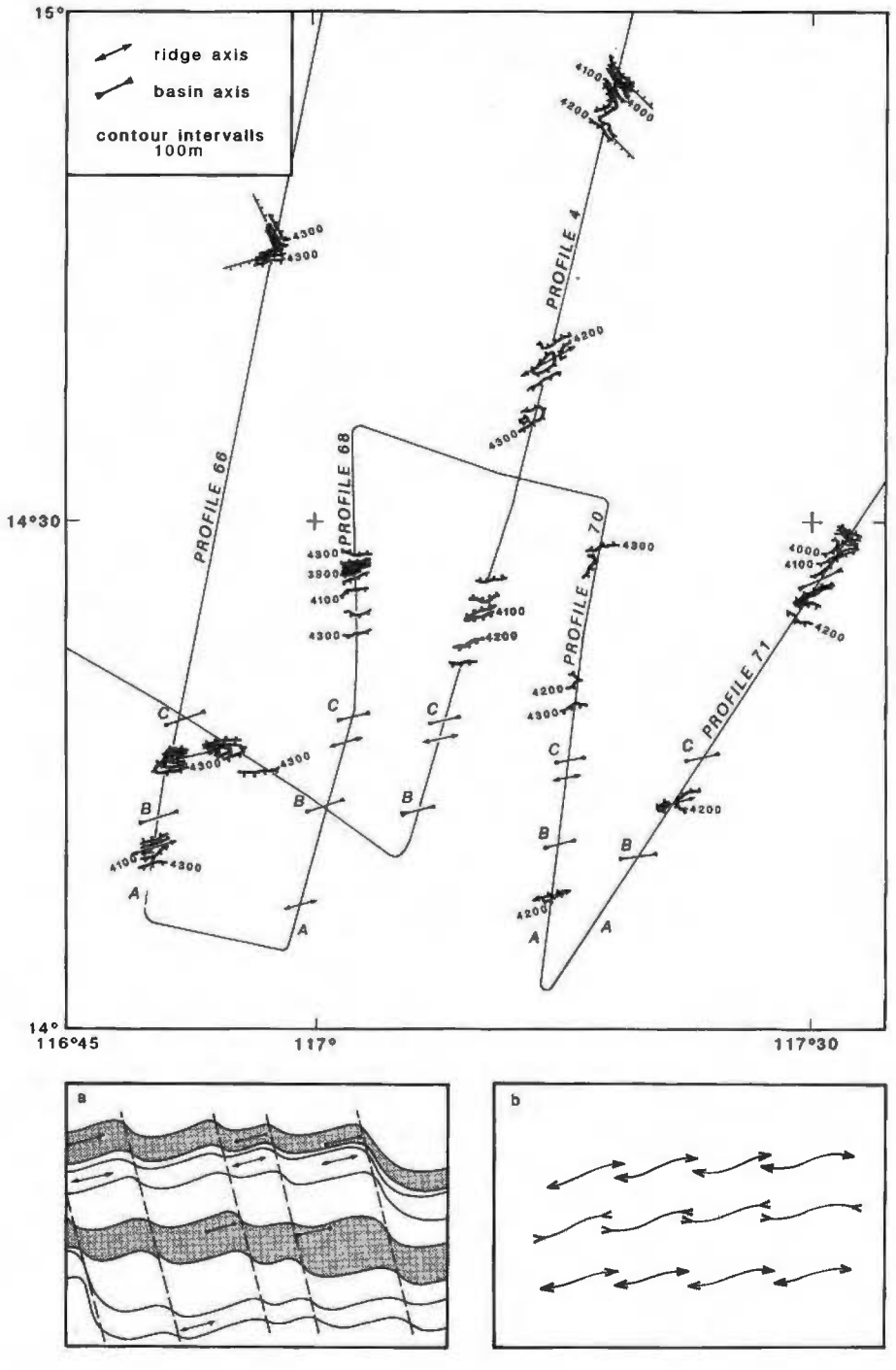

Figure 10

Bathymetry and structure of the southern detailed study area. The Seabeam coverage reveals discontinous ridges. Interpretation based on Seabeam data combined with seismic profiles of Figure 11. *Bottom sketches are two alternative interpretations a: series of transform faults. Basins in grey b: overlapping spreading centers.*

Représentation de la bathymétrie et des orientations structurales sur les routes de la zone détaillée B (position sur la fig. 4). Le grain structural est constitué de collines allongées N 80°E, séparées par des vallées. Ces collines et vallées sont discontinues (A, B, C) et paraissent être disposées en échelon. *a* et *b* sont des hypothèses pour expliquer cette disposition. *a* : présence de failles transformantes nombreuses et à faible coulissage; *b* : centres de distension à recouvrement (OSC).

CONCLUSIONS

The Seabeam and geophysical survey conducted at the SCS ridge axis answers several questions concerning the geodynamic evolution of this marginal basin. It also raises new ones.

Among the answered questions is the structural continuity of the axial ridge throughout the South China Sea. The fabric of the seafloor in the 200 km-wide axial region is characterized by outward-tilted blocks, limited by normal faults trending N 50-60°E. This structural continuity suggests that the oceanic basin in the Southwest abyssal plain may be coeval with the last event of spreading further east. A preliminary model of the magnetic anomalies suggests a synchronous cessation of the spreading between 113 and 120°E, just after magnetic anomaly 5 *c* (16 My).

The complex morphological pattern of the central section of this ridge, between 155°E and 118°E, is the result of the transection of the axis by numerous N

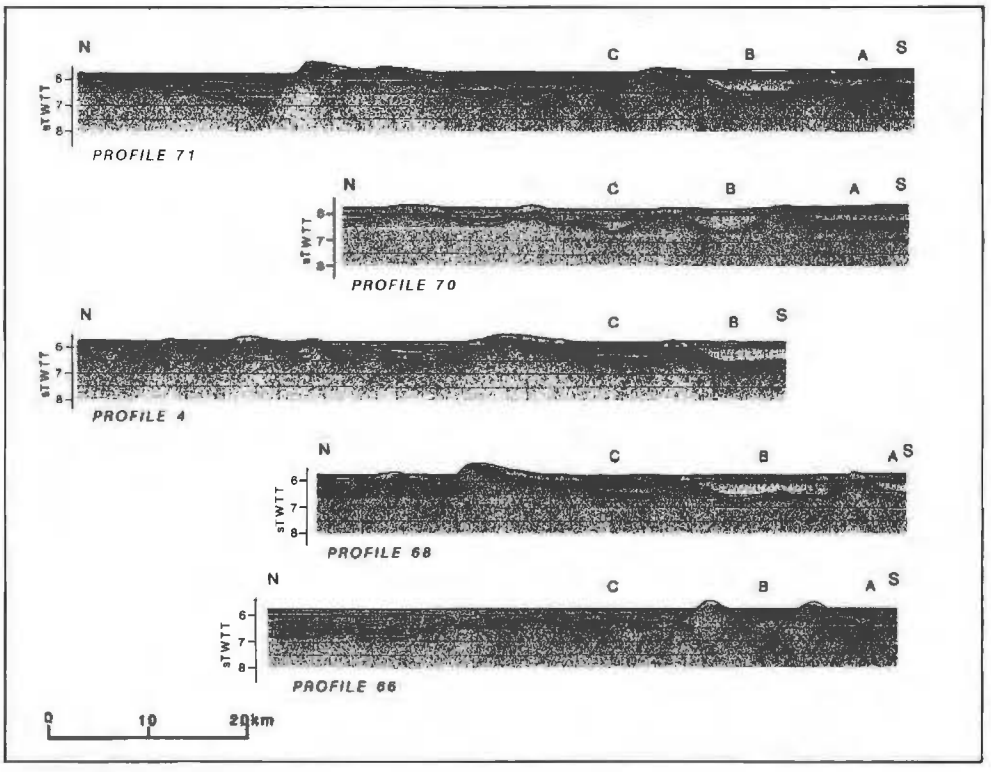

Figure 11

Interpreted seismic profiles across the southern detailed area. Profiles located on Figure 10. *Correlation of the different troughs (A, B and C) based on thickness and distribution of sedimentary sequences.*

Profils sismiques interprétés dans la zone B (position fig. 10). La corrélation des bassins A, B et C a été faite d'après la morphologie et la succession stratigraphique.

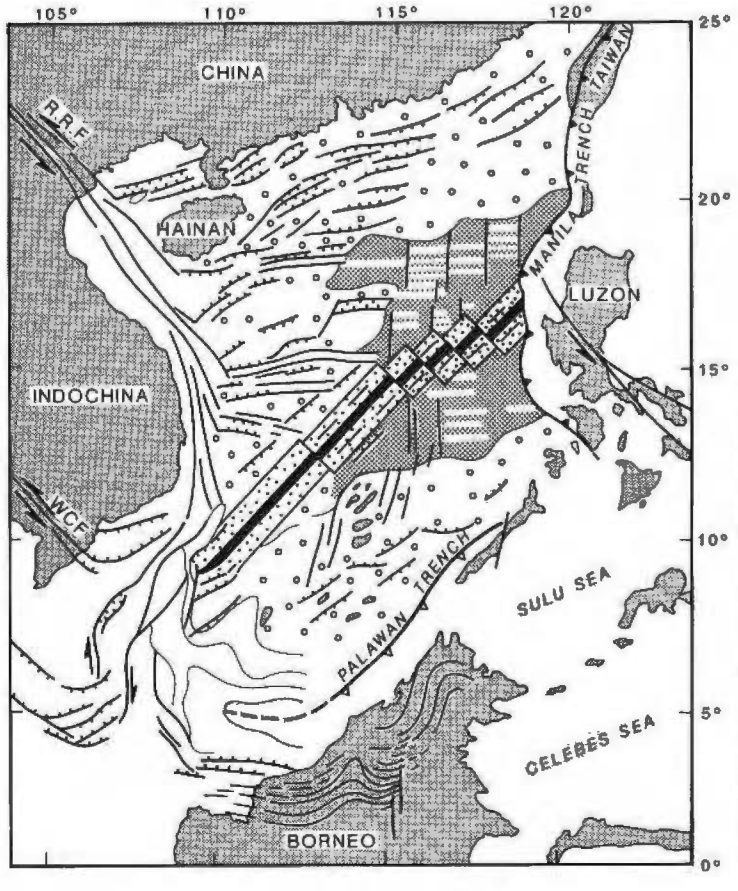

Figure 12

The history of the SCS presented in tectonic sketch map. Modified from Tapponnier et al. (1986) *and Pautot et al.* (1986). *The Palawan trench is interpreted as an inactive subduction zone. Stretched continental margins of the basin (open circles) are affected by both East-West and Northeast-Southwest trending normal faults. The complex West boundary includes the Red River fault, and the extension at sea of the Wang Chao (WCF) and Three Pagodas (TPF) faults. Oldest oceanic crust* (32-20 *My*) *in grey. White lines are East-West magnetic anomalies. Dotted area is most recent oceanic crust* (20-14 *My*).

Structure schématique du bassin de Chine méridionale. Ce schéma est une modification des figures de Pautot *et al.* (1986) et Tapponnier *et al.* (1986). La fosse de Palawan est interprétée comme une zone de subduction fossile. Les marges continentales amincies sont affectées de cercles ouverts, et on a représenté les principaux linéaments d'orientation générale Est-Ouest et Nord-Est-Sud-Ouest. Sur le continent asiatique : RRF = faille de la Rivière Rouge; WCF = faille de Wang Chao. La croûte océanique ancienne (32-20 Ma) est représentée en gris, et les lignes blanches sont les anomalies magnétiques Est-Ouest. La zone centrale avec le pointillé représente la croûte océanique récente (20-14 Ma).

140°E trending transform faults. Numerous seamounts were injected at the end of the spreading (Scarborough Seamount chain) preferentially along these transform faults, as evidenced by Seabeam. The geochemical data obtained on these seamounts support the alkalic signature of this post-spreading volcanism previously reported by Taylor and Hayes (1983).

Another important result is the quite homogeneous structural trend (N 50-N 60°E) all along the central part of the axial ridge. Additional rift structures oriented N 70-N 80°E were also detected along both edges of the surveyed area, suggesting a spreading reorganization.

Difficulties arise when we try to accomodate the N 50-N 60°E trend of the axial ridge structures with our observations of N 80°E structures and the East-West trending magnetic anomalies (11 to 6 *a*) of the eastern oceanic basin (Taylor ans Hayes, 1980; 1983).

One way to explain this discrepancy is to assume that the whole oceanic basin is transected in a right lateral sense by numerous N 140°E trending transform faults (Briais *et al.*, in press). If we extend a N 50-70°E rift fabric off the axis, and if we assume that the magnetic anomalies follow the same trend, the East-West trend reported by Taylor and Hayes (1980; 1983) only exists at the overall scale of the basin, as for the East-West orientation of the Scarborough seamount chain. This interpretation is valid only in light of the widely-spaced profiles presently published. However, the magnetic anomalies map recently compiled by Chen (1987), presenting 15-20 km spaced profiles, suggests a good consistency of the East-West magnetic lineations in the eastern basin, and consequently would not allow extending the N 50-70°E fabric off-axis.

Another way to reconcile the orientation of the magnetic lineations and the structural observations is to suggest that the direction of spreading rotated 20 or 30° counterclockwise about 20 My ago (Fig. 12). This is documented along the southeastern flank of the ridge where closely-space profiles show N 80°E trending structures changing to N 60°E toward the axis, and on the northern flank of the northeastern ridge section (Figs. 4, 10). The stretched continental margins of the basin are affected by both East-West and Northeast-Southweast trending normal faults. These two extensional directions are also inferred in the oceanic crust, with related transform faults.

According to the first interpretation, the whole South China Sea would have opened with a Northwest-Southeast direction of extension. This would be compatible with Tertiary left lateral movements along large strike-slip faults such as the Red River fault in China and the Wang Chao and Three Pagodas faults in Sundaland. Rifts trending Northwest-Southeast could have formed at the tips of those strike-slip faults. The spreading would have followed the same structural directions, with possible 10 to 20° variations in the orientation of the ridge segments. In this case, the South China Sea could be the direct consequence of extrusion of the Indochina block in response to the India-Asia continental collision (*e. g.*, Tapponnier *et al.*, 1986).

The second interpretation implies a change in the direction of spreading, which might be related to a significant kinematic reorganization around 20 My. According to this hypothesis, the oldest oceanic crust (32-20 My) is limited to the eastern part of the basin, where East-West magnetic anomalies are offset by probable North-South trending transform faults. It was created during the Oligo-Miocene spreading stage in the South China Sea, independant of the India-Asia collision, but related to a general East-est spreading event, which also occurred to the North, in the Japan Sea and the Yellow Sea (Jolivet, 1986). The most recent oceanic crust trends Northeast-Southwest all across the basin, parallel to the Palawan trench, and is dissected by N 140 transform faults. We favour this interpretation implying a 20 to 30° counter-clock wise rotation of the rift axis with a general kinematic neorganization around 20 My.

Acknowledgements

This work was the result of a cooperative program (*Nanhai*) conducted in the South China Sea between the French government and the People's Republic of China. We thank all participants, particularly Commandant Hubert Guidal and the crew, for collaboration on board *R/V Jean-Charcot*. Special thanks go to K. Feigl for reviewing earlier versions of this paper.

REFERENCES

Batiza R. and D. Vanko (1983). Volcanic development of small oceanic central volcanoes on the flank of the East Pacific rise inferred from narrow beam echo sounder survey. *Mar. Geol.*, **54**, 53-90.

Ben Avraham Z. and S. Uyeda (1973). The evolution of the China basin and the Mesozoic paleogeography of Borneo. *Earth planet. Sci. Letts*, **18**, 365-376.

Bowin C., R. Lu, C. Lee and H. Schouten (1978). Plate convergence and accretion in the Taiwan Luzon region, *Am. Ass. Petrol. Geol. Bull.*, **62**, 1645-1672.

Briais A., P. Tapponnier and G. Pautot (in press). Constraints of Seabeam data on crustal fabric and seafloor spreading in the South China Sea. *Earth planet. Sci. Letts.*

Chen S. (1987). Map of magnetic profiles, in: *Atlas of Geology and Geophysics of South China Sea*, 1:2 000 000, He L. and B. Chen Editors, Guangzhou Marine Geological Exploration Company Limited.

Fricaut L. (1984). Étude géologique et structurale de la marge Nord Palawan. *Thèse de 3e cycle*, Université de Paris XI.

Hayes D. E., S. Spangler, W. Zeng, B. Yao, B. Taylor and A. Briais (1987). Age and evolution of the South China Sea southwest subbasin. *Eos Trans., AGU Annual Meeting, Abstr.*, **68**, 1496.

Hékinian R., P. Bonté, G. Pautot, D. Jacques, L. Labeyrie, N. Mikkelsen and J.-L. Reyss (1989). Volcanics from the South China Sea ridge system. *Oceanologica Acta*, **12**, 2, 101-115.

Hinz K. and H. U. Schlüter (1985). Geology of the Dangerous Grounds, South China Sea, and the continental margin off Southwest Palawan: Results of Sonne cruises SO-23 and SO-27. *Energy*, **10**, 297-315.

Holloway N. (1982). North Palawan block, Philippines: its relation to Asian mainland and role in evolution of the South China Sea, *Bull. Am. Ass. Petrol. Geol.*, **66**, 1355-1383.

Jolivet L. (1986). America-Eurasia plate boundary in eastern Asia and the opening of marginal basins. *Earth planet. Sci. Letts*, **81**, 282-288.

Lu W., C. Ke, J. Wu, J. Liu and C. Lin (1987). Characteristics of magnetic lineations and tectonic evolution of the South China Sea basin. *Acta oceanol. sin.*, **6**, 4, 577-588.

Patriat P. (1983). L'évolution cénozonique du système de dorsale de l'Océan Indien. *Thèse d'État, Université Paris-VI.*

Pautot G., C. Rangin, A. Briais, P. Tapponnier, P. Beuzart, G. Lericolais, X. Mathieu, J. Wu, S. Hann, H. Li, Y. Lu and J. Zhao (1986). Spreading direction in the Central South China Sea. *Nature*, **321**, 150-154.

Pautot G. and C. Rangin (1989). Subduction of the South China Sea axial ridge below Luzon (Philippines); Underplating process along an oblique convergent margin. *Earth planet. Sci. Letts*, **92**, 57-69.

Peltzer G. (1983). Naissance et évolution des décrochements lors d'une collision continentale, approche expérimentale, application à la tectonique de l'Est de l'Asie. *Thèse de 3e cycle, Université Paris-VII.*

Rangin C. and J. Francheteau (1980). Fine scale morphological and structural analysis of the East Pacific Rise, 21°N (RITA project). *Proceedings 26th International Geological Congress, Geology of oceans symposium.* Paris, 7-17 July, 1980. *Oceanologica Acta*, n° sp., 15-24.

Ru K. and J.D. Pigott (1986). Episodic rifting and subsidence in the South China Sea. *Am. Ass. Petrol. Geol. Bull.*, **70**, 1136-1155.

Tapponnier P., G. Peltzer and R. Armijo (1986). On the mechanics of the collision between India and Asia, in: *Collision tectonics*, M. P. Coward and A. C. Ries, editors, Geol. Soc. Spec. Publ., 19, 115-157.

Taylor B. and D. E. Hayes (1980). The tectonic evolution of the South China Basin, in: The tectonic and geologic evolution of Southeast Asian seas and islands, D. E. Hayes, editor. *Geophys. Monogr. Am. geophys. Un.*, **vol. 23,** Washington, D.C., 89-104.

Taylor B. and D. E. Hayes (1983). Origin and history of the South China Basin, in: The tectonic and geologic evolution of Southeast Asian seas and islands: part 2, D. E. Hayes, editor. *Geophys. Monogr. Am. geophys. Un.*, **vol. 27,** Washington, D.C., 23-56.